Vietnam Journal of Earth Sciences, 40(4), 354-366, Doi: 10.15625/0866-7187/40/4/13106

(VAST)

Vietnam Academy of Science and Technology

Vietnam Journal of Earth Sciences

http://www.vjs.ac.vn/index.php/jse

Determination of maximum tilt angle from analytic signal amplitude of magnetic data by the curvature-based method

Pham Thanh Luan[1], Le Huy Minh[2], Erdinc Oksum[3], Do Duc Thanh[1]*

[1]*VNU, Hanoi - University of Science, Faculty of Physics, Department of Geophysics, Ha Noi, Vietnam*

[2]*Institute of Geophysics, Vietnam Academy of Science and Technology, Hanoi, Vietnam*

[3]*Süleyman Demirel University, Engineering Faculty, Department of Geophyisical Engineering, 32260 Isparta, Turkey*

Received 04 April 2018; Received in revised form 10 August 2018; Accepted 08 September 2018

ABSTRACT

Imaging buried geological boundaries is one of a major objective during the interpretation of magnetic field data in Geophysics. Therefore, edge detection and edge enhancement techniques assist a crucial role on this aim. Most of the existing edge detector methods require to obtain special points such as in general the maxima of the resulting image. One of the useful tools in estimating edges from magnetic data is the tilt angle of the analytical signal amplitude due to its value slightly dependence on the direction of magnetization. In this study, the maxima of the tilt angle of analytical signal amplitudes of the magnetic data was determined by a curvature-based method. The technique is based on fitting a quadratic surface over a 3×3 windows of the grid for locating any appropriate critical point that is near the centre of the window. The algorithm is built in Matlab environment. The feasibility of the algorithm is demonstrated in two cases of synthetic data as well as on real magnetic data from Tu Chinh-Vung May area. The source code is available from the authors on request.

Keywords: the curvature-based method; tilt angle; analytic signalamplitude; edge detection; Tu Chinh-Vung May.

1. Introduction

One of the important tasks of magnetic interpretation is to determine the locations and lateral boundaries of anomalous bodies. Many methods have been used to solve this problem. The horizontal gradient method (Cordell, 1979; Cordell and Grauch, 1985) is the simplest and common approach to detect edges. The biggest advantage of the method is its low sensitivity to the noise in the data because it only requires the first order horizontal derivatives of the field. However, the horizontal gradient method requires a reduction to the pole or pseudogravity transformation that is notoriously unstable at low magnetic latitudes. Wijns et al. (2005) proposed the theta map method that can be applied to magnetic anomalies at low latitudes for delineating magnetic contacts. Although the shallow geological boundaries are clear and refined, the geologi-

*Corresponding author, Email: doducthanh1956@gmail.com

cal boundaries at deeper levels are clear but diffuse (Chen et al., 2017). Nabighian (1972) and Roest et al. (1992) presented another widely used method to locate the lateral edges of source bodies by using the position of maxima of analytic signal amplitude. In 2D case, the shape of the analytic signal amplitude is independent of the direction of the source magnetization vector. However, in 3D case, Li (2006) demonstrated that the analytic signal amplitude is not independent of the direction of the ambient magnetic field and the direction of magnetization. Hsu et al. (1996) proposed an enhanced analytic signal method, which uses the high order derivatives to locate the lateral edges of source bodies on the grid plane. They pointed out that higher order analytic signal can effectively reduce the interference effects due to adjacent bodies and can outline the horizontal boundaries of geological bodies precisely and clearly, but increase the effect of noise. Cooper (2014) proposed a modified analytic signal amplitude that based on tilt angle method of Miller and Singh (1994) for the direct interpretation of magnetic anomalies. The advantage of the method is reducing the dependence of the analytic signal amplitude of magnetic anomaly on the direction of magnetization.

The above methods operate with functions that tend to have maxima located over the edges of the causative magnetic body. A simple method widely used for the automated detection of these maxima is based on the approach of Blakely and Simpson (1986). The method finds the location of maxima by fitting a parabola to three successive data points. Most existing research employ either this method to determine fault locations (Hsu et al., 1996; Vo et al., 2005; Beiki., 2010; Nguyen et al., 2014; Akpınaret al., 2016; etc). Another method also used to determine the maximum was introduced by Phillips et al. (2007), called it the curvature-based method. Although both methods examine 3×3 arrays over the data grid, Blakely and Simpson's method analyze a set of 1D sections through the window, whereas Phillips et al.'s analysis is 2D. The method was applied to find the maximum of the horizontal gradient, analytic signal amplitude and local wavenumber (Phillips et al., 2007).

In this paper, we will locate the horizontal boundaries of geological bodies by using locations of the maximum amplitude of the tilt angle of the analytic signal amplitude of magnetic data. The locations will be detected by the curvature-based method. The application of the presented algorithm is shown on a real magnetic dataset from Tu Chinh-Vung May area.

2. Theory

The definition of the analytic signal amplitude of magnetic anomaly M is given by Nabighian (1972) and Roest et al. (1992) as follows:

$$A=\sqrt{\left(\frac{\partial M}{\partial x}\right)^2+\left(\frac{\partial M}{\partial y}\right)^2+\left(\frac{\partial M}{\partial z}\right)^2} \quad (1)$$

Li (2006) showed that the amplitude of the analytic signal is not independent of magnetization vector direction for the general 3D case. A modified analytic signal amplitude that has a much-reduced dependence on the source vector direction is introduced by Cooper (2014), called the tilt angle of analytic signal amplitude:

$$T=\tan^{-1}\left(\frac{\dfrac{\partial A}{\partial z}}{\sqrt{\left(\dfrac{\partial A}{\partial x}\right)^2+\left(\dfrac{\partial A}{\partial y}\right)^2}}\right) \quad (2)$$

Because the tilt angle is based on the ratio of derivatives, it enhances both large and small analytic signal amplitude well. The locations of the maximum of the tilt angle can be automatically determined by the curvature-based method that was introduced by Phillips et al. (2007) for aeromagnetic interpretation. The method involves passing a 3×3 window over the data grid and locating any appropriate critical point that is near the center of the window. The first step in locating the maximum is to solve within each window for the coefficients of the quadratic surface passing through the nine data points of the window.

$$A + Bx + Cy + Dx^2 + Exy + Fy^2 \approx g\left(x, y\right) \quad (3)$$

Using a local coordinate system with its origin at the center $g_{i,j}$ of the window (Figure 1), the coefficients of the quadratic surface can be determined by linear least-squares method:

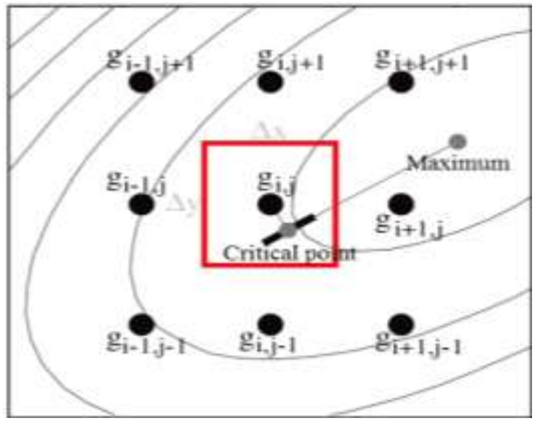

Figure 1. The quadratic surface that fit the nine data points, and its maximum and critical point (modified from Phillips et al., 2007)

$$A = \frac{1}{9}\left[5g_{i,j} + 2\left(g_{i+1,j} + g_{i-1,j} + g_{i,j+1} + g_{i,j-1}\right) - \left(g_{i+1,j+1} + g_{i+1,j-1} + g_{i-1,j-1}\right)\right]$$

$$B = \frac{1}{6\Delta x}\left[g_{i+1,j+1} + g_{i+1,j} + g_{i+1,j-1} - \left(g_{i-1,j+1} + g_{i-1,j} + g_{i-1,j-1}\right)\right]$$

$$C = \frac{1}{6\Delta y}\left[g_{i+1,j+1} + g_{i,j+1} + g_{i-1,j+1} - \left(g_{i+1,j-1} + g_{i,j-1} + g_{i-1,j-1}\right)\right]$$

$$D = \frac{1}{3\left(\Delta x\right)^2}\left[g_{i+1,j+1} + g_{i+1,j} + g_{i+1,j-1} + g_{i-1,j+1} + g_{i-1,j} + g_{i-1,j-1} - 2\left(g_{i,j+1} + g_{i,j} + g_{i,j-1}\right)\right]$$

$$E = \frac{1}{4\Delta x\Delta y}[g_{i+1,j+1} + g_{i-1,j-1} - g_{i+1,j-1} - g_{i-1,j+1}]$$

$$F = \frac{1}{3\left(\Delta y\right)^2}\left[g_{i+1,j+1} + g_{i,j+1} + g_{i-1,j+1} + g_{i+1,j-1} + g_{i,j-1} + g_{i-,j-1} - 2\left(g_{i+1,j} + g_{i,j} + g_{i-1,j}\right)\right] \quad (4)$$

where Δx and Δy are the width of the intervals in the x and y directions, respectively. At the location of the extremum (x_e, y_e) of the quadratic surface, the partial derivatives satisfy $\frac{\partial g}{\partial x}(x_e, y_e) = 0$ and $\frac{\partial g}{\partial y}(x_e, y_e) = 0$, thus

$$\begin{cases} x_e = \dfrac{2FB - CE}{E^2 - 4DF} \\ y_e = \dfrac{2CD - BE}{E^2 - 4DF} \end{cases} \quad (5)$$

Where the denominator is zero, the surface can be a plane, a ridge or a trough, and therefore has no unique extremum. Associated with the quadratic surface is Hessian matrix H that is obtained by taking the second order partial derivatives of $g\left(x, y\right)$.

$$\begin{pmatrix} \dfrac{\partial^2 g}{\partial x^2} & \dfrac{\partial^2 g}{\partial x \partial y} \\ \dfrac{\partial^2 g}{\partial x \partial y} & \dfrac{\partial^2 g}{\partial y^2} \end{pmatrix} = \begin{pmatrix} 2D & E \\ E & 2F \end{pmatrix} \quad (6)$$

The eigenvalues λ of the Hessian matrix are:

$$\begin{aligned} \lambda_+ &= \left(D + F\right) + \sqrt{\left(D - F\right)^2 + E^2}, \\ \lambda_- &= \left(D + F\right) - \sqrt{\left(D - F\right)^2 + E^2} \end{aligned} \quad (7)$$

Using the eigenvalues, the types of extremum and the dominant elongation of a quadratic surface can be determined as Table1. Here, we only consider the cases the surface contains a maximum and the maximum lies along a ridge (The cases 1 and 2).

Table 1. The type of extremum and the dominant elongation of a quadratic surface

Cases	λ_-	λ_+	$\lvert\lambda_-\rvert / \lvert\lambda_+\rvert$	Extremum	Dominant elongation	Location
1	< 0	< 0		Maximum	Ridge	x_e, y_e
2	< 0	> 0	> 1	Saddle point	Ridge	x_0, y_0
3	< 0	> 0	< 1	Saddle point	Trough	
4	> 0	> 0		Minimum	Trough	

In the first case, the location of the maximum (x_e, y_e) will be determined by Eq. (6). In the second case, the location of the critical point (x_0, y_0) can be calculated by using the following equation:

$$\begin{cases} x_0 = -\dfrac{Be_{>x}^2 + Ce_{>x}e_{>y}}{2\left(De_{>x}^2 + Ee_{>x}e_{>y} + Fe_{>y}^2\right)} \\ y_0 = -\dfrac{Be_{>x}e_{>y} + Ce_{>y}^2}{2\left(De_{>x}^2 + Ee_{>x}e_{>y} + Fe_{>y}^2\right)} \end{cases} \tag{8}$$

Where $e_> = (e_{>x}, e_{>y})$ is an eigenvector of the eigenvalue λ_-. The eigenvector is given by:

$$\begin{pmatrix} e_{>x} \\ e_{>y} \end{pmatrix} = \begin{cases} \begin{pmatrix} 1 \\ (\lambda_- - 2D)/E \end{pmatrix} or \begin{pmatrix} (\lambda_- - 2F)/E \\ 1 \end{pmatrix} if\ E \neq 0 \\ \begin{pmatrix} 1 \\ E/(\lambda_- - 2F) \end{pmatrix} if\ \lambda_- \neq 2F \\ \begin{pmatrix} E/(\lambda_- - 2D) \\ 1 \end{pmatrix} if\ \lambda_- \neq 2D \end{cases} \tag{9}$$

We note here that to avoid duplicate solutions, the result for any window should be accepted only if the maximum or critical point lies within the red box (with sizes Δx and Δy horizontally) about the centre of the window (Figure 1).

3. Synthetic example

The efficiency of the tilt angle of the analytic signal amplitude and the curvature-based method to determine the edges of the causative body is studied by analysis of two synthetic examples.

The first example involves a single prism model with parameters shown in Table 2. The magnetic anomaly due to the prism obtained from the application of Rao and Babu (1991) method is shown in Figure 2. The outline of the prismatic source is also shown by the black lines in Figure 2. Obviously, when the direction of magnetization is not vertical, the magnetic anomaly isn't located directly above the source body. Figure 3c shows the tilt angle of the analytic signal amplitude of the magnetic anomaly. It can be observed from this figure that the tilt angle enhances all edges of the source body, and the locations of its maxima can be used to locate the lateral edges of the source. The maxima are located by the curvature-based method (Figure 3d). As can be seen in Figure 3d, the detected edges of the causative bodies based on the maxima of the tilt angle of the analytic signal amplitude are located over the true boundaries (the black lines).

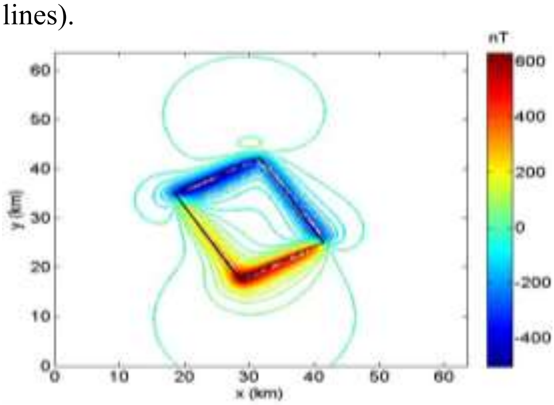

Figure 2. Synthetic magnetic anomaly of the single prism model

Table 2. Parameters of the single prism model

Center coordinates (km; km)	30; 30
Inclination I (^{o})	30
Declination D (^{o})	0
Magnetization (A/m)	5
Length × Width (km)	20×15
Depth of top (km)	1
Depth of bottom (km)	2
Rotation angle (^{o})	60

To assess the edge detection results of the tilt angle of the analytic signal amplitude, we compared our result with the analytic signal amplitude (Roest et al., 1992) and another method based on the horizontal gradient of the vertical derivative of the magnetic anomaly. Figure 3a shows the analytic signal amplitude. It can be seen that the analytic signal amplitude is only effective in enhancing two of the four edges of the source. Figure 3b shows the horizontal gradient of the vertical derivative of the magnetic anomaly. Clearly, the method cannot well extract the edges, and it brings some false edges surrounding the real edges. From Figure 3a, b, and c, it can be seen that the tilt angle has the best results relative to the other edge recognition methods.

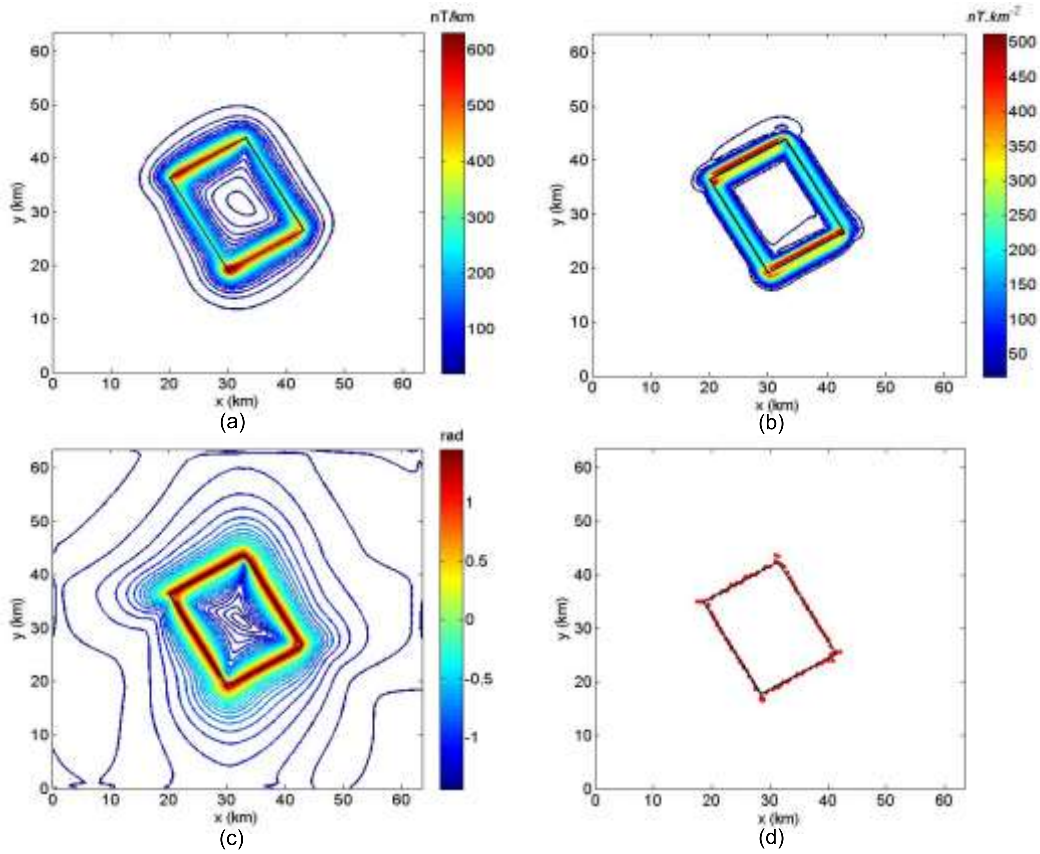

Figure 3. Test results of the single prism model
(a) The analytic signal amplitude, (b) The horizontal gradient of vertical derivative, (c) The tilt angle of the analytic signal amplitude, (d) ● ● ●: The maxima of the tilt angle of the analytic signal amplitude

The second example is more complex. The observed anomaly is the superposition of effects from different sources. The example involves two prisms with low magnetic inclinations, one is close to the surface (the thinner and longer prism), and another is located beneath the first and therefore it is partially hidden. Parameters of two sources are given in Table 3.

Table 3. Parameters of the two prism model

Parameters	Prism 1	Prism 2
Center coordinates (km; km)	31.5; 31.5	31.5; 31.5
Inclination I (°)	6	5
Declination D (°)	0	0
Magnetization (A/m)	4	5
Length × Width (km)	70×1.5	30×15
Depth of top (km)	0.3	0.7
Depth of bottom (km)	0.7	1.5
Rotation angle (°)	45	-45

Figure 4 shows a magnetic anomaly due to these prisms. The outlines in the plan view of the prismatic sources are also displayed in Figure 4 (the black lines). Using this field, the tilt angle of the analytic signal amplitude is calculated and shown in Figure 5a. Then, by applying the curvature-based method, we obtain the location of maxima (Figure 5b). It can be observed that, in spite of the interference effects from neighboring source, the algorithm can outline the edges precisely and clearly. The hidden part of the deeper source is also located on the grid plane.

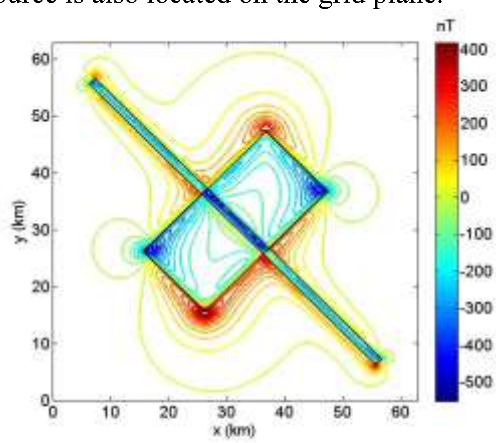

Figure 4. Synthetic magnetic anomaly of two prisms

In order to test the stability of the algorithm, random noise with the amplitude equal to 2% of the anomaly amplitude was added to the data. Here, we note that, to reduce the noise effect, upward continuation of 0.2 km is used prior to calculations of the tilt angle. Figure 5c shows the result of the tilt angle of the analytic signal amplitude when the random noise had been added. It can be clearly seen in Figure 5d that the edge detection results, in this case, compares very favorably with the theoretical model (the black lines).

4. Real data example

The practical applicability of the algorithm is demonstrated with the interpretation of magnetic anomalies from Tu Chinh-Vung May area. The study area covers an area of approximately 49000 km^2, in an area defined in latitude by the interval 75°-95°N and in longitude by 110°-112°E (Figure 6). The area is located in the deepwater area of the southern part of Vietnam's Eastern Sea, but during the Eocene to Pliocene, it was formed in continental, coastal, shallow marine and bay-lagoonal environments (Tran Nghi, 2017). The geological development history of the area is closely related with generation and evolution of the East sea, composed of following periods: pre-rift, syn-rift, post-rift and shelf generation periods (Le Duc Cong, 2015). The ages of the sediments range from Eocene to Oligocene. The seismic profiles showed that filled sediments estimated about 7-8km thick at the depocenter. The structure of area was separated into complex blocks by NE-SW and EW faults (Nguyen et al., 2014).

Figure 6 also shows the total field magnetic anomaly from Tu Chinh - Vung May area, that was interpreted by Nguyen et al. (2014). The magnetic anomaly values vary from -250 to + 150nT in the study area, with many positive and negative anomalies that have E-W trend.

Remanent magnetization of mid-ocean ridge basalt is the major source of magnetic anomalies in the East Vietnam Sea. Since the study area is positioned within a low latitude region, reduction to the pole or pseudo - gravity transformation is not advisable.

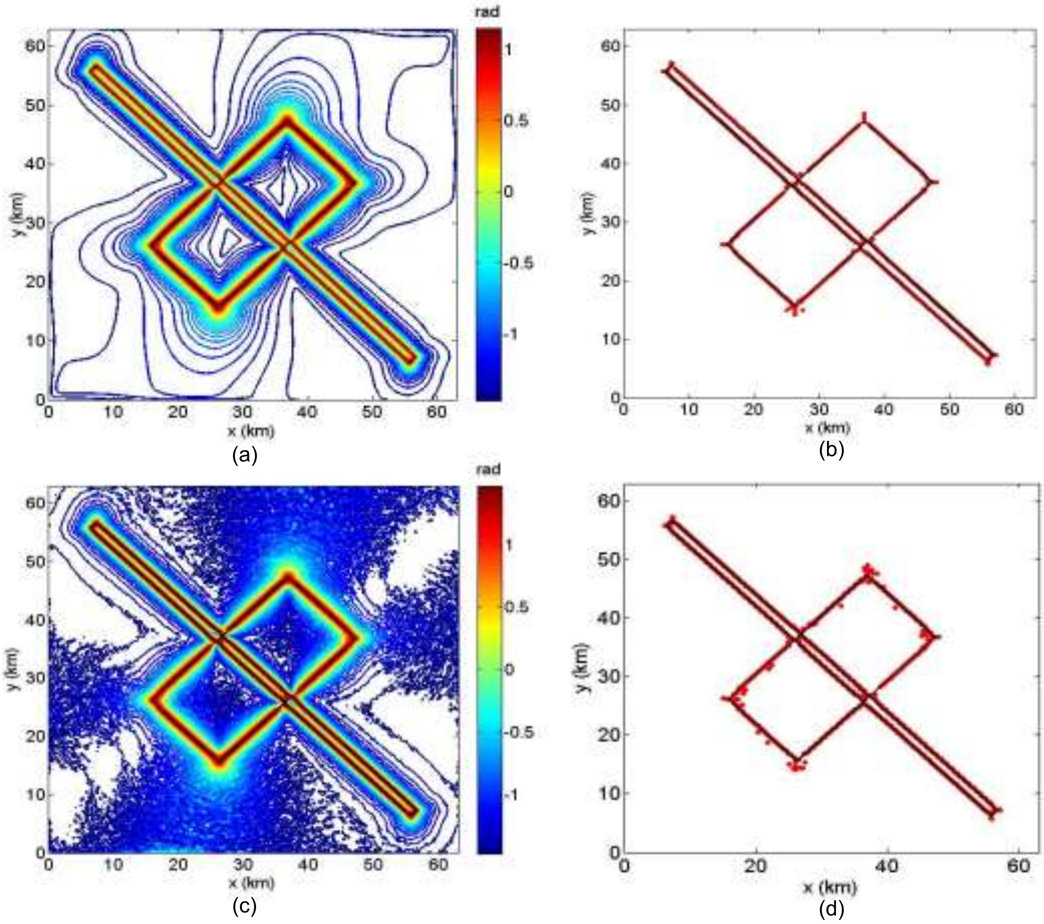

Figure 5. Test results of the two prism model

(a) The tilt angle of the analytic signal amplitude, (b) ● ● ●: The maxima of the tilt angle of the analytic signal amplitude, (c) The tilt angle of the analytic signal amplitude with the random noise, (d) ● ● ●: The maxima of the tilt angle of the analytic signal amplitude with the random noise

Before the boundary detection processing, the upward continuation of the total field magnetic anomaly was performed to filter out the effects of near-surface heterogeneities that may not be of primary geological interest. Here, we performed the boundary detection of magnetic sources at different upward continuation heights, including 2.5 km, 5.0 km, and 7.5 km. The upward continuation also produced results that are smoother and less sensitive to random noise than the original anomaly, but will not change the primary shapes. Figure 7 shows the result of determining the tilt angle of the analytic signal amplitude and its maxima at upward continuation level of 5 km. Clearly, the tilt angle is effective in bringing out the details of the small amplitude anomalies because it is based on the ratio of derivatives. Therefore, the application of the curvature-based method to the tilt angle can give a detailed and clear boundaries detection result on the grid plan, as shown in Figure 7.

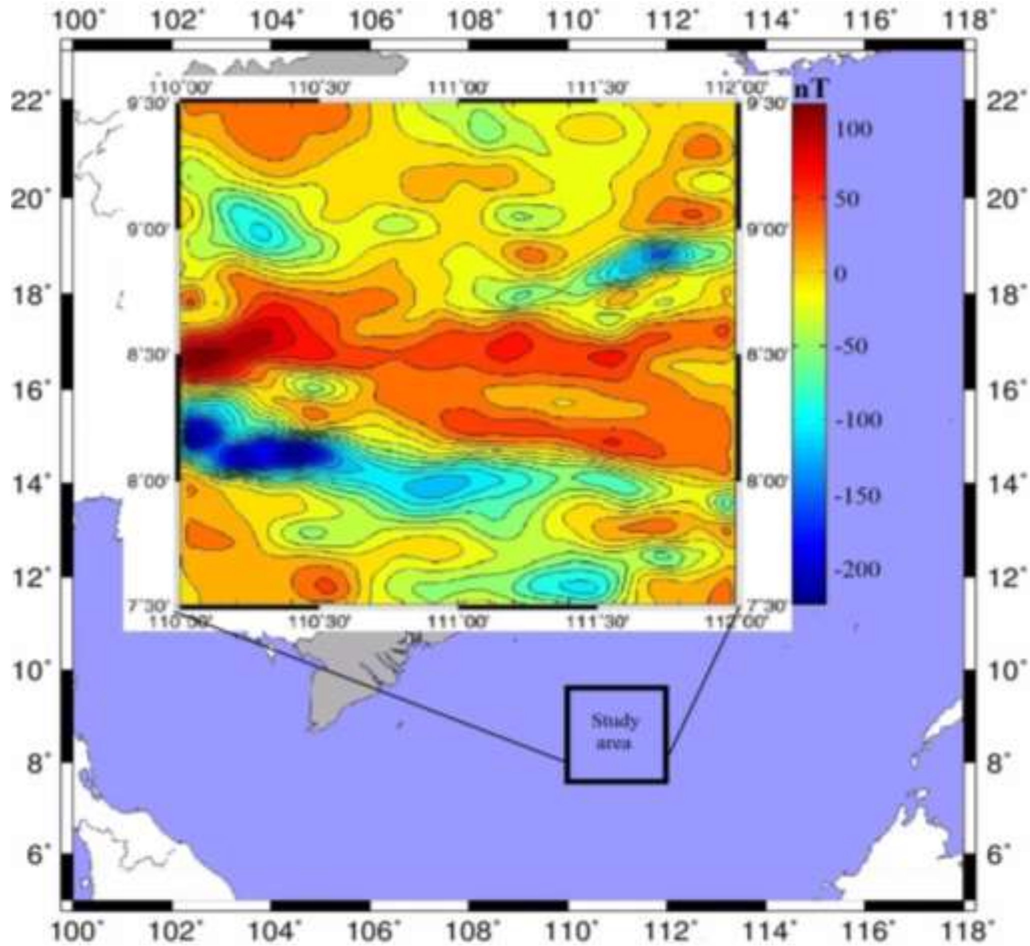

Figure 6. The total field magnetic anomaly and location map of the study area

Using the results of locating the maxima of the tilt angle of analytic signal amplitude at three different levels of upward continuation (Figure 8), the magnetic boundaries are obtained and shown in Figure 9. Comparing the results of locating the maxima of the tilt angle of the analytic signal amplitude at three different levels of upward continuation (Figure8) and the faults determined by Nguyen et al. (2014) based on magnetic boundaries obtained from the horizontal gradient of the magnetic anomaly and the horizontal gradient of the vertical gradient of the magnetic anomaly (Figure 8), we can see that, besides several results that coincide with E-W, ENE-WSW and NWN-SES trending faults, the presented method further indicates many other magnetic boundaries. This can be explained due to using the horizontal gradient of the magnetic anomaly, and the horizontal gradient of the vertical derivative of the magnetic anomaly cannot display the strong and weak amplitude anomaly edges simultaneously, as discussed in the theory section and tested on a synthetic example. Furthermore, the use of the horizontal gradient methods for original magnetic anomaly cannot accurately determine the boundary of the magnetic sources. To further confirm the results, we also compared the magnetic boundaries obtained from the presented algorithm and faults that based on seismic data (Figure 9). Figure 10 and 11 show two seismic sections reported by Nguyen et al. (2014) and Tran et al. (2018), respectively.

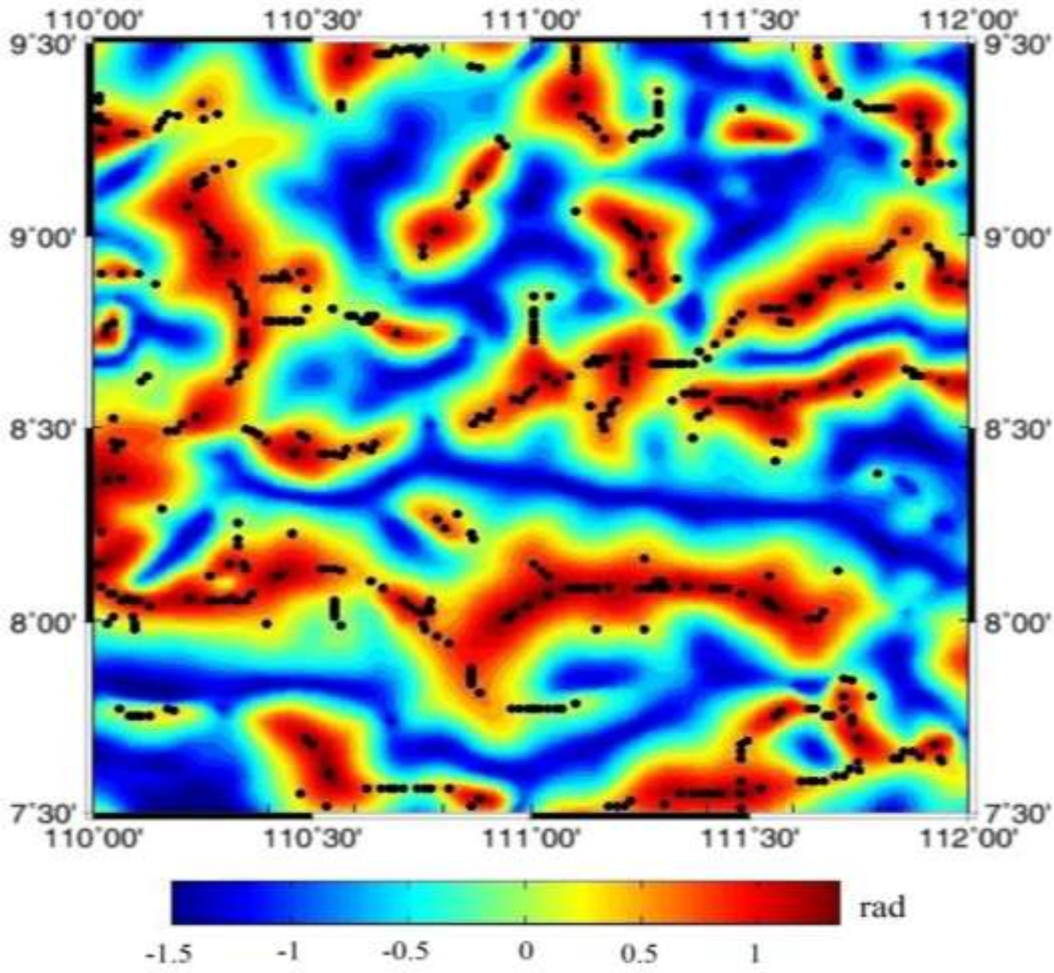

Figure 7. The tilt angle of the analytic signal amplitude and its maxima at upward continuation level of 5 km

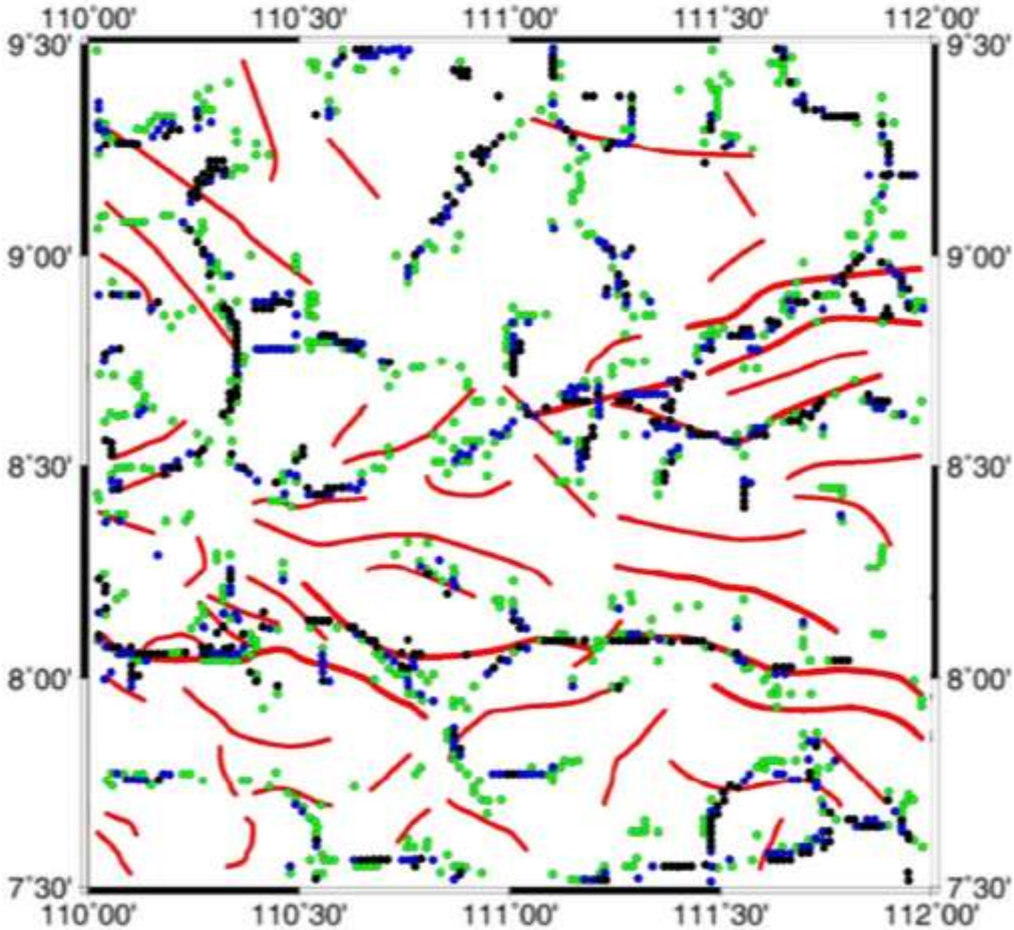

Figure 8. The maxima of tilt angle of analytic signal amplitude at three different levels of upward continuation
: The maxima at upward continuation level of 2.5km,
: The maxima at upward continuation level of 5km,
: The maxima at upward continuation level of 7.5km)
: The fault systems (after Nguyen et al., 2014)

It can be clearly observed from these figures that there are many faults that were determined by interpreting the seismic data. And although the presented algorithm cannot outline all faults on the seismic lines and A'B', most of the magnetic boundaries that the algorithm generated are in agreement with the faults obtained from the seismic analysis. The faults coincide with the magnetic boundaries are marked 1, 2, 3, 4, 5 along the seismic line AB and 1', 2', 3', 4', 5' along the seismic line AB (Figure 9). Thus, it can be confirmed that the magnetic boundaries that found using the presented algorithm can be used as a good reference for locating faults in the study area, so making an improved geological interpretation possible.

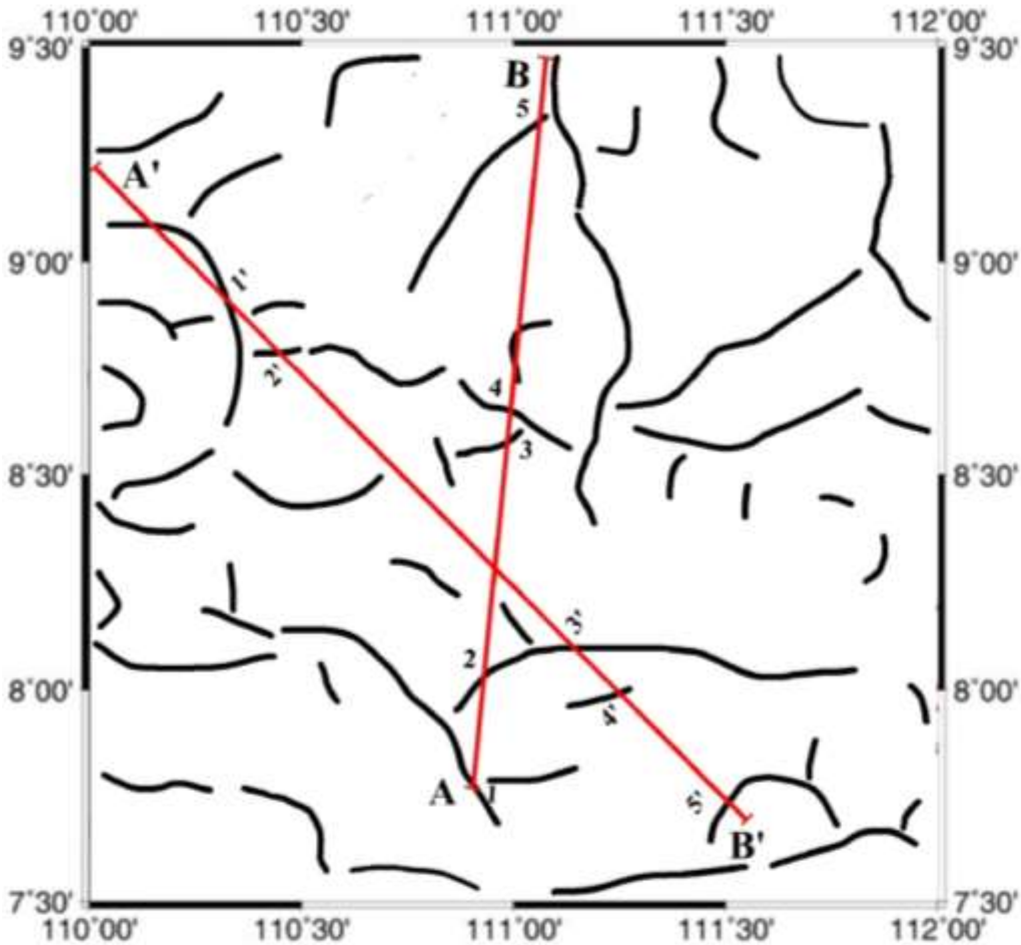

Figure 9. The magnetic boundaries of the study area

A ⊢⊣ B, A' ⊢⊣ B': The seismic lines   1 – 5, 1' – 5': The fault location coincides with the magnetic boundary

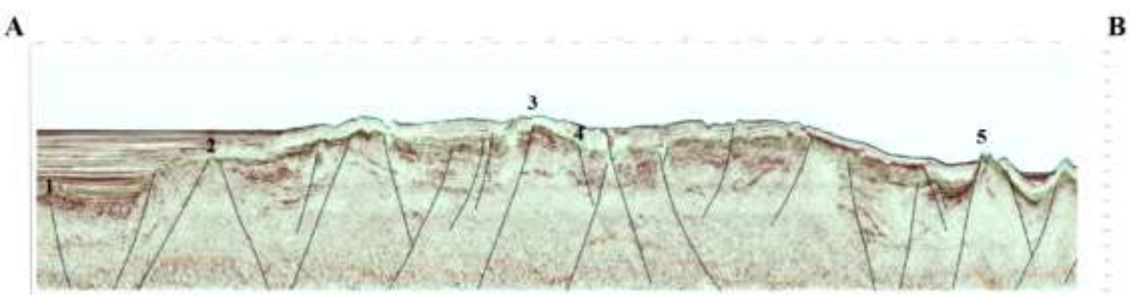

Figure 10. Interpreted seismic section of line A-B in study area (after Nguyen et al., 2014)

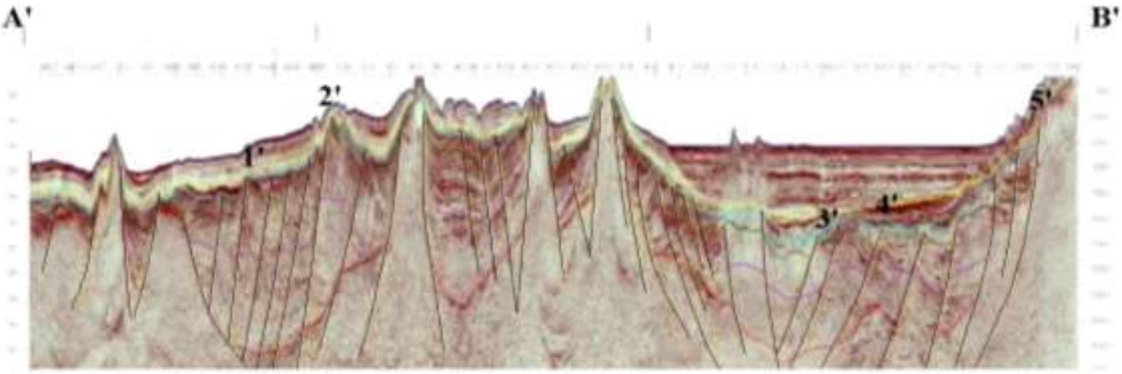

Figure 11. Interpreted seismic section of line A'-B' in study area (after Tran et al., 2018)

5. Conclusions

We developed a program using an algorithm that based on the tilt angle of the analytic signal amplitude and the curvature-based method to detect the edges of causative bodies. Findings showed that the boundaries of geological bodies are enhanced more accurately using the presented algorithm, compared with the other methods. Synthetic test cases also showed that the results of the boundary detection are adequately stable even in the case of interference from neighboring sources. The algorithm is applied to a real magnetic data from Tu Chinh - Vung May area. The results showed that the magnetic boundaries that found using the presented algorithm can be used as a good reference for the geological structure interpretation of the area. Additionally, it must be noted that in the areas where the level of noise is high, using upward continuation can help reduce the effects of noise and increase the coherency of the solutions.

Acknowledgments

We thank the editor and two reviewers for helpful comments on the manuscript. This research is funded by the VNU University of Science under project number TN.18.05.

References

Akpınar Z., Gürsoy H., Tatar O., Büyüksaraç A., Koçbulut F., Piper, JDA., 2016. Geophysical analysis of fault geometry and volcanic activity in the Erzincan Basin, Central Turkey, Complex evolution of a mature pull-apart basin. Journal of Asian Earth Sciences, 116, 97-114.

Beiki M., 2010. Analytic signals of gravity gradient tensor and their application to estimate source location, Geophysics, 75(6), 159-174.

Blakely R. J., and Simpson R.W., 1986. Approximating edges of source bodies from magnetic or gravity anomalies, Geophysics, 51, 1494-1498.

Chen An-Guo, Zhou Tao-Fa, Liu Dong-Jia, Zhang Shu, 2017. Application of an enhanced theta-based filter for potential field edge detection: a case study of the LUZONG ORE DISTRICT, Chinese Journal of Geophysics, 60(2), 203-218.

Cooper G.RJ., 2014. Reducing the dependence of the analytic signal amplitude of aeromagnetic data on the source vector direction, Geophysics, 79, 55-60.

Cordell L., 1979. Gravimetric Expression of Graben Faulting in Santa Fe Country and theEspanola Basin, New Mexico. In Ingersoll, R.V., Ed., Guidebook to Santa Fe Country, New Mexico Geological Society, Socorro, 59-64.

Cordell L and Grauch V.J.S., 1985. Mapping Basement Magnetization Zones from Aeromagnetic Data in the San Juan Basin, New Mexico, The Utility of Regional Gravity and Magnetic Anomaly Maps, Society of Exploration Geophysicists, Tulsa, 181-197.

Hsu S.K., Coppense D., Shyu C.T., 1996. High- resolution detection of geologic boundaries from potential field anomalies: An enhanced analytic signal technique, Geophysics, 61, 1947-1957.

Le D.C., Application of seismic exploration methods to identify geological structural characteristics supporting for hydrocarbon potential assessment in Tu-Chinh - Vung May basin, Ph.D. Thesis, Hanoi University of Mining and Geology.

Li X., 2006. Understanding 3D analytic signal amplitude: Geophysics, 71(2), 13-16.

Miller H.G. and Singh V., 1994. Potential Field Tilt a New Concept for Location of Potential Field Sources, Journal of Applied Geophysics, 32, 213-217.

Nabighian M.N., 1972. The analytic signal of two-dimensional magnetic bodies with polygonal cross-section: Its properties and use of automated anomaly interpretation, Geophysics, 37, 507-517.

Nguyen N.T., Bui V.N., Nguyen T.T.H., 2014. Determining the depth to the magnetic basement and fault systems in Tu Chinh - Vung May area by magnetic data interpretation, Journal of Marine Science and Technology, 14(4a), 16-25.

Nguyen X.H, San T.N, Bae W., Hoang M.C, 2014. Formation mechanism and petroleum system of tertiary sedimentary basins, offshore Vietnam, Energy Sources, Part A, 36, 1634-1649.

Phillips J.D., Hansen R.O. and Blakely R.J., 2007. The use of curvature in potential-field interpretation, Exploration Geophysics, 38(2), 111-119.

Rao D.B., and Babu N.R., 1991. A rapid method for three-dimensional modeling of magnetic anomalies, Geophysics, 56(11), 1729-1737.

Roest W.R., Verhoef J., and Pilkington M., 1992. Magnetic interpretation using the 3-D analytic signal, Geophysics, 57, 116-125.

Tran N., 2017. Sediment geology of Vietnam, VNU Press.

Tran T.D., Tran N., Nguyen T.H., Dinh X.T., Pham B.N., Nguyen T.T., Tran T.T.T.N., Nguyen T.H.T., 2018. The Miocenedepositional geological evolution of Phu Khanh, Nam Con Son and Tu Chinh - Vung May basins in Vietnam continental shelf, VNU Journal of Science: Earth and Environmental Sciences, 34(1), 112-135.

Vo T.S., Le H.M., Luu V.H., 2005. Three-dimensional analytic signal method and its application in interpretation of aeromagnetic anomaly maps in the Tuan Giao region, Proceedings of the 4th geophysical scientific and technical conference of Vietnam, Publisher of Science and Engineering 2005.

Wijns C, Perez C and Kowalczyk P, 2005, Theta map: Edge detection in magnetic data, Geophysics, 70, 39-43.